Severe Skin Permeability Barrier Dysfunction in Knockout Mice Deficient in a Fatty Acid ω-Hydroxylase Crucial to Acylceramide Production

Masatoshi Miyamoto[1,2], Narumi Itoh[1,2], Megumi Sawai[1], Takayuki Sassa[1], and Akio Kihara[1]

[1]Laboratory of Biochemistry, Faculty of Pharmaceutical Sciences, Hokkaido University, Kita 12-jo, Nishi 6-chome, Kita-ku, Sapporo 060-0812, Japan

[2]These authors contributed equally to this work.

Correspondence:

Akio Kihara

Laboratory of Biochemistry, Faculty of Pharmaceutical Sciences

Hokkaido University

Kita 12-jo, Nishi 6-chome, Kita-ku, Sapporo 060-0812, Japan

Tel: +81-11-706-3754

Fax: +81-11-706-4900

E-mail: kihara@pharm.hokudai.ac.jp

Short title: Skin barrier dysfunction due to ω-hydroxylase deficiency

ORCIDs:

Masatoshi Miyamoto, 0000-0002-7785-7438

Narumi Itoh, 0000-0002-1307-8777

Megumi Sawai, 0000-0002-7406-802X

Takayuki Sassa, 0000-0003-3145-9829

Akio Kihara, 0000-0001-5889-0788

Abbreviations: ARCI, autosomal recessive congenital ichthyosis; SB, stratum basale; SC, stratum corneum; SG, stratum granulosum; SS, stratum spinosum; CIE, congenital ichthyosiform erythroderma; CYP, cytochrome P450; E, embryonic day; FA, fatty acid; HI, harlequin ichthyosis; KLK, kallikrein-regulated peptidase; KO, knockout; LC-MS/MS, liquid chromatography coupled with tandem mass spectrometry; LI, lamellar ichthyosis; ω-OH, ω-hydroxy; RT, reverse transcription; TEWL, transepidermal water loss; TLC, thin-layer chromatography; ULC, ultra-long-chain; WT, wild type

ABSTRACT

The skin permeability barrier is indispensable for maintaining water inside the body and preventing the invasion of pathogens and allergens; abnormalities lead to skin disorders such as atopic dermatitis and ichthyosis. Acylceramide is an essential lipid for skin barrier formation, and CYP4F22 is a fatty acid ω-hydroxylase involved in its synthesis. Mutations in *CYP4F22* cause autosomal recessive congenital ichthyosis, although the symptoms vary among mutation sites and types. Here, we generated knockout mice deficient in *Cyp4f39*, the mouse ortholog of human *CYP4F22*, to investigate the effects of completely abrogating the function of the fatty acid ω-hydroxylase involved in acylceramide production on skin barrier formation. *Cyp4f39* knockout mice died within 8 h of birth. Large increases in transepidermal water loss and penetration of a dye from outside the body were observed, indicating severe skin barrier dysfunction. Histological analyses of epidermis revealed impairment of lipid lamellae formation, accumulation of corneodesmosomes in stratum corneum, and persistence of periderm. In addition, lipid analyses by mass spectrometry showed almost complete loss of acylceramide and its precursor ω-hydroxy ceramide. In conclusion, our findings provide clues to the molecular mechanisms of skin barrier abnormalities and the pathogenesis of ichthyosis caused by *Cyp4f39*, and *CYP4F22* by association.

INTRODUCTION

The skin permeability barrier ("skin barrier" below) prevents the invasion of foreign substances such as pathogens, allergens, and chemicals into the body, as well as loss of water from the body. Impairment of the skin barrier causes various skin disorders, such as ichthyosis, atopic dermatitis, and infections. Ichthyosis is one type of hyperkeratosis and is characterized by dryness and scaling of the skin (Oji et al, 2010). Skin is composed of epidermis, dermis, and subcutaneous tissue: the epidermis is further divided, from the surface downward, into stratum corneum (SC), stratum granulosum (SG), stratum spinosum (SS), and stratum basale (SB). The skin barrier is mainly formed in the SC. Lipids can prevent the permeation of substances due to their high hydrophobicity. In the SC, corneocytes are surrounded by a multi-layered lipid structure, called the lipid lamellae, which play a central role in skin barrier function (Kihara, 2016). The lipid lamellae are mainly composed of ceramides, cholesterols, and fatty acids (FAs). Of the various ceramide classes, acylceramide (ω-*O*-acylceramide) is epidermis-specific and is a so-called "barrier lipid" specialized for skin barrier formation (Hirabayashi et al, 2019; Kihara, 2016).

Ceramide is the hydrophobic backbone of sphingolipids, one of the major lipid components of eukaryotic membranes (Kihara, 2016). It has two hydrophobic chains, a long-chain base and an FA, which form an amide bond. Acylceramide, however, is unique in that it has three hydrophobic chains wherein linoleic acid is esterified to the ω position of the FA moiety (Figure 1a). In addition, its FA chain is unusually long: mainly C30–36, compared with C16–24 for normal ceramides (Kihara, 2016). FAs can be classified according to chain length into long-chain (C11–C20) and very-long-chain (≥C21); chains of ≥C26 are sometimes called ultra-long-chain (ULC) (Kihara, 2012, 2016). The structural characteristics of acylceramide are important

for the formation and maintenance of lipid lamellae, and abrogation of acylceramide production leads to defective lipid lamellae formation and causes ichthyosis (Hirabayashi et al, 2019; Kihara, 2016). Some of the acylceramide is converted into protein-bound ceramide through modification of its linoleic acid moiety, subsequent hydrolysis, and covalent bonding with corneocyte surface proteins (Supplementary Figure S1) (Hirabayashi et al, 2019; Kihara, 2016). Protein-bound ceramide is a major constituent of the cell surface, a solid membrane structure termed the corneocyte lipid envelope, assumed to play an essential role in connecting the lipid lamellae with keratinocytes (Elias et al, 2014).

Congenital ichthyosis is classified into several types according to the symptoms and causative genes, of which autosomal recessive congenital ichthyosis (ARCI) is characterized by the most severe symptoms (Oji et al, 2010; Sugiura & Akiyama, 2015). ARCI is further divided into harlequin ichthyosis (HI), lamellar ichthyosis (LI), congenital ichthyosiform erythroderma (CIE), in order of symptom severity. To date, ten genes have been identified as causative of ARCI (Hotz et al, 2018; Sugiura & Akiyama, 2015), of which three (*CERS3*, *CYP4F22*, and *PNPLA1*) are involved in acylceramide synthesis (Hirabayashi et al, 2019; Kihara, 2016), and two (*ALOXE3* and *ALOX12B*) are involved in the conversion of acylceramide to protein-bound ceramide (Supplementary Figure S1) (Zheng et al, 2011). Mutations in these genes cause LI or CIE (Sugiura & Akiyama, 2015), and mutations in other genes involved in acylceramide production (*ELOVL1*, *ELOVL4*, and *ABHD5*) cause syndromic types of ichthyoses (Aldahmesh et al, 2011; Kutkowska-Kazmierczak et al, 2018; Mueller et al, 2019; Ohno et al, 2018; Sassa et al, 2013; Vasireddy et al, 2007). Except for *CYP4F22*, knockout (KO) mice deficient in each of these acylceramide-related genes have already been created and analyzed (Grond et al, 2017; Hirabayashi et al, 2017; Jennemann et al, 2012;

Pichery et al, 2017; Radner et al, 2010; Sassa et al, 2013; Vasireddy et al, 2007): all exhibit neonatal lethality due to skin barrier abnormalities, confirming the important role of acylceramide in skin barrier formation.

CYP4F22 is one of the ~50 members of the cytochrome P450 (CYP) family in humans. We recently revealed that CYP4F22 is an FA ω-hydroxylase that catalyzes the hydroxylation of the ω position of ULCFAs in the acylceramide synthetic pathway based on cellular and biochemical analyses (Figure 1a) (Ohno et al, 2015). Mutations in this gene in ARCI patients were first reported in 2006 (Lefèvre et al, 2006); to date, over 40 have been documented (Hotz et al, 2018). Affected individuals do not all exhibit identical skin symptoms, although they are often born with signs of erythroderma—or in some cases, as collodion babies— and are later diagnosed with mild LI or CIE. However, acylceramide levels have only been measured in one ichthyosis patient, who had mild symptoms (Ohno et al, 2015). The patient has residual CYP4F22 activity, so although their acylceramide level is greatly reduced relative to normal levels, it is not zero. Currently, the relationships among the *CYP4F22* mutation types, enzyme activity levels, and ARCI symptoms remain mostly unclear. In the present study we generated and analyzed the skin phenotype of KO mice deficient in *Cyp4f39*, the mouse ortholog of human *CYP4F22*, as a model of ARCI with completely abrogation of FA ω-hydroxylase function in acylceramide synthesis.

RESULTS

Skin barrier abnormalities in *Cyp4f39* KO mice

There are six and nine CYP4F subfamily members in human and mouse, respectively. The phylogenetic tree of these proteins shows that mouse Cyp4f39 is most closely related to human CYP4F22 (Figure 1b), suggesting that mouse Cyp4f39 is a functional homolog of human CYP4F22. Indeed, mouse Cyp4f39 shares 86.4% identity and 93.7% similarity with human CYP4F22. To elucidate the effect of FA ω-hydroxylase deficiency on the skin barrier in living organisms and on ARCI symptoms, we generated *Cyp4f39* KO mice using the CRISPR/Cas9 system. A target sequence was set in exon 11, and we obtained *Cyp4f39* KO mice with a 32 bp frameshift deletion (Figure 1c). No *Cyp4f39* KO mice survived beyond the day of birth, suggesting that the mutation is neonatal lethal, as is the case for KO mice deficient in other genes involved in acylceramide synthesis (Hirabayashi et al, 2019; Kihara, 2016). The skin of *Cyp4f39* KO mice extracted on embryonic day 18.5 (E18.5) by cesarean section was more erythematous, shinier, and less wrinkled than that of wild type (WT) mice (Figure 1d). This phenotype resembles the symptoms observed in human ARCI patients with *CYP4F22* mutations (Hotz et al, 2018).

We examined the survival time courses of $Cyp4f39^{+/+}$, $Cyp4f39^{+/-}$, and $Cyp4f39^{-/-}$ mice following birth by cesarean section. All the $Cyp4f39^{+/+}$ and $Cyp4f39^{+/-}$ mice survived for more than 15 h (Figure 2a). In contrast, all $Cyp4f39^{-/-}$ (*Cyp4f39* KO) mice died within 8 h. Next, we examined the change in body weight following birth by cesarean section. While $Cyp4f39^{+/+}$ and $Cyp4f39^{+/-}$ mice had maintained 98% of their birth weight 7 h after birth, $Cyp4f39^{-/-}$ mice lost weight rapidly, to only 67% of their birth weight at 7 h (Figure 2b). To investigate the cause of this drop, we measured transepidermal water loss (TEWL). $Cyp4f39^{-/-}$ mice had a TEWL value

14.8 times higher than that of *Cyp4f39*$^{+/+}$ mice (Figure 2c), indicating that the rapid body weight loss observed in *Cyp4f39* KO mice is due to increased transpiration of water from the body. We also performed a toluidine blue-staining assay. While little staining was observed in the control *Cyp4f39*$^{+/-}$ mice, thorough staining was observed in *Cyp4f39* KO mice (Figure 2d). In summary, the skin barrier function of *Cyp4f39* KO mice is severely impaired, which lead to neonatal lethality.

Impaired lipid lamellae formation and persistence of periderm in *Cyp4f39* KO mice

Histological analysis by hematoxylin/eosin staining was conducted on WT and *Cyp4f39* KO mouse epidermis. Gaps were observed in the SC of WT mice (Figure 3a). These gaps correspond to the lipid lamellae in the living body, washed away by organic solvents during the deparaffinization and dehydration steps of the staining procedure. In contrast, there were almost no gaps in the SC of *Cyp4f39* KO mice, suggesting that these mice possessed few lipid lamellae to begin with.

The epidermal structure was examined in more detail using transmission electron microscopy. In *Cyp4f39* KO mouse epidermis, the lipid lamellae were thinner than in WT mice (Figure 3b and c). *Cyp4f39* KO mice had slightly more SC layers than WT mice (Figure 3d), and thicker corneocytes as well. In addition, persistent periderm was observed on the outermost layer of the *Cyp4f39* KO mouse epidermis (Figure 3b, Supplementary Figure S2a). Under normal conditions, the periderm covering the immature epidermis of the fetus disappears as the epidermis matures and the SC forms. Many corneodesmosomes were observed in the SC of *Cyp4f39* KO mice (Figure 3b and e, Supplementary Figure S2b), structures involved in cell adhesion that under normal conditions would disappear from the upper layer of the SC.

Lipids constituting the lipid lamellae are synthesized in the region from the upper SS to the SG and stored in lamellar bodies. These bodies' interiors appear granular at first, but gradually transform into multilayer lamellar 'stacks' as they approach the top of the SG (i.e. the boundary between the SG and the SC) (Narangifard et al, 2018). The lamellar bodies eventually fuse with cell membranes in the top of the SG, and the stored lipids are released extracellularly, processed, and incorporated into the lipid lamellae (Hirabayashi et al, 2019; Kihara, 2016). Acylceramide is stored in the lamellar bodies in the form of acyl-glucosylceramide and then reconverted into acylceramide after it has been released to the outside of the corneocytes. In the epidermis of WT mice, multilayer, mature lamellar bodies were observed at the boundary between the SG and the SC (Figure 3b, green arrowheads). In contrast, only small, immature, granular lamellar bodies existed in the *Cyp4f39* KO mice, suggesting that the immaturity of the lamellar bodies impaired the formation of lipid lamellae, which in turn causes skin barrier dysfunction.

Almost complete loss of acylceramide in *Cyp4f39* KO mice

To compare the lipid composition of WT and *Cyp4f39* KO mouse epidermis, lipids were extracted from the epidermis of E18.5 mice, separated by thin-layer chromatography (TLC), and then stained using a copper phosphate reagent. Lipid bands for acylceramide and its derivative acyl-glucosylceramide were absent from lanes containing samples from *Cyp4f39* KO mice (Figure 4a). On the other hand, ULC species of ceramides and glucosylceramides were more strongly represented. There were no apparent differences in the abundances of other lipids between WT and *Cyp4f39* KO mice.

The quantity of each acylceramide species (as defined by chain length and saturation status [saturated or monounsaturated] of the FA moiety) was measured using liquid chromatography-

coupled with tandem mass spectrometry (LC-MS/MS). WT mouse epidermis contained substantial amounts of saturated C30–C34 and monounsaturated C32–C36 acylceramides (Figure 4b). However, almost no acylceramides were observed for *Cyp4f39* KO mice, total acylceramide content reaching only 1.5% of that of WT mice. This indicates that Cyp4f39 is nearly the only FA ω-hydroxylase involved in acylceramide synthesis in mice.

Decreased ω-hydroxy (ω-OH) ceramides and increased ULC ceramides in *Cyp4f39* KO mice

In the acylceramide synthetic pathway, Cyp4f39 catalyzes the reaction upstream of the production of the acylceramide intermediate ω-OH ceramide (Supplementary Figure S1). We measured ω-OH ceramide levels using LC-MS/MS. Saturated and monounsaturated C30–C36 ω-OH ceramides (Figure 5a) were observed in WT mouse epidermis (Figure 5b). However, *Cyp4f39* KO mice had little, only ~5.4% of WT levels of total species.

Lipid analysis by TLC showed a higher proportion of ULC ceramides among ceramide species in *Cyp4f39* KO than in WT epidermis (Figure 4a). We performed a more detailed analysis of the ceramide species (Figure 5c) using LC-MS/MS. In the WT epidermis, C26:0 ceramide was most abundant, followed by C24:0 and C26:1 ceramides (Figure 5d). Although *Cyp4f39* KO mouse epidermis had lower quantities of some ≤C28 ceramides, such as C22:0, C26:0, C26:1, and C28:1, than did WT epidermis, it did contain substantial amounts of ≥C30 ceramides (C32–C36 saturated and C34–C36 monounsaturated), which were almost absent in WT mice. It is likely that ≥C30 ULCFAs, which would normally be used for acylceramide production after ω-hydroxylation by Cyp4f39, were instead incorporated into ceramides in *Cyp4f39* KO epidermis.

Weak effects of *Cyp4f39* disruption on expression of keratinocyte-differentiation markers and acylceramide synthesis genes

Mutations in genes involved in acylceramide production can affect the gene expression of keratinocyte-differentiation markers and other acylceramide synthesis genes (Grond et al, 2017; Hirabayashi et al, 2017; Sassa et al, 2013). The effect of *Cyp4f39* disruption on gene expression was examined using quantitative real-time reverse transcription (RT)-PCR. The expressions of *Krt14* (keratin 14; SB marker) and *Krt10* (keratin 10; SS and SG marker) in *Cyp4f39* KO mice were similar to those in WT mice (Figure 6). However, the expression of *Flg* (filaggrin), a marker of the SG, was higher. The expressions of two other SG markers, *Lor* (loricrin) and *Ivl* (involucrin), were slightly elevated in *Cyp4f39* KO mice, although this difference was not statistically significant. Of the genes involved in acylceramide synthesis (*Elovl1*, *Elovl4*, *Cers3*, *Pnpla1*, and *Abhd5*), only *Elovl4* and *Cers3* had slightly higher expression in *Cyp4f39* KO mice. Expressions of neither *Aloxe3*—the gene encoding lipoxygenase, which is involved in the production of protein-bound ceramides— nor *Abca12*—the gene encoding an ATP-binding cassette transporter, which transports lipids to lamellar bodies—were changed in *Cyp4f39* KO mice compared with WT mice. Overall, the gene expressions of keratinocyte-differentiation markers and acylceramide/protein-bound ceramide–related genes were not strongly affected by *Cyp4f39* disruption, although there were some weak effects.

DISCUSSION

In the present study, *Cyp4f39* KO mice were created and analyzed as a pathological model of complete loss of FA ω-hydroxylase function. The skin of these mice was erythematous (Figure 1d), which resembles the erythrodermic symptoms observed at birth in human ARCI patients with *CYP4F22* mutations (Hotz et al, 2018). Mice also exhibited very severe skin barrier abnormalities, and all died within 8 h of birth (Figure 2). Their TEWL value was 14.8 times that of WT mice. Only slight hyperkeratosis was observed in the mutant mice (Figure 3). *Cyp4f39* KO mice showed thickening of the corneocytes, impaired lipid lamellae formation, and persistence of periderm (Figure 3, Supplementary Figure S2). Although periderm is a different structure from the collodion membranes observed in some ichthyosis patients, it is possible that there may be a similar mechanism for the abnormal persistence of periderm and collodion membranes, such as the involvement of undegraded corneodesmosomes. Desmosomes are modified and transformed into corneodesmosomes during the differentiation of keratinocytes into corneocytes. Corneodesmosomes are degraded in the upper layer of the SC, mainly by kallikrein-family proteases (kallikrein-regulated peptidases; KLKs), resulting in desquamation (Ishida-Yamamoto & Igawa, 2014). In the present study, we found that many corneodesmosomes remained undegraded throughout the SC of *Cyp4f39* KO mice (Figure 3, Supplementary Figure S2), as was seen in *Cers3* KO mice; *Cers3* encodes ceramide synthetase, which is involved in acylceramide synthesis (Jennemann et al, 2012). These residual corneodesmosomes may be related to the persistence of periderm and the pathogenesis of ichthyosis. In fact, mutations in the gene encoding matriptase (*ST14*), which converts pro-KLKs to mature KLKs, cause impairment of corneodesmosome degradation, resulting in ichthyosis (Basel-Vanagaite et al, 2007). The proteases that degrade corneodesmosomes are regulated by

protease inhibitors, pH, and cholesterol sulfate (Chan & Mauro, 2011; Deraison et al, 2007; Elias et al, 2004; Ishida-Yamamoto & Igawa, 2014). In the upper layer of the SC, pH is lowered by several factors, including FAs, lactic acid from eccrine glands, and amino acids and urocanic acid derived from filaggrin, among others (Chan & Mauro, 2011; Krien & Kermici, 2000). KLKs are inhibited by the protease inhibitor lymphoepithelial Kazal-type inhibitor, and low pH induces activation of KLKs by promoting dissociation from the inhibitor (Deraison et al, 2007). Although the mechanism by which corneodesmosomes remain undegraded in *Cyp4f39* KO mice is unclear, defective lipid lamellae formation may alter the localization or orientation of lipids such as FAs and cholesterol sulfate, resulting in abnormal regulation of protease activity. Lamellar bodies contained lamellar stacks in WT mice, but not in *Cyp4f39* KO mice, in which they were rather granular (Figure 3b). Under normal conditions, the granular interior of the lamellar bodies undergoes transition to a lamellar stack near the top of the SG (Narangifard et al, 2018). However, this process seems to have been impaired in the *Cyp4f39* KO mice. The characteristic structure of acylceramide may thus be important for the formation and maintenance of the lamellar stack morphology.

Acylceramides were almost completely absent from the epidermis of *Cyp4f39* KO mice (Figure 4). A similar near-complete absence of acylceramide has been observed in *Pnpla1* KO mice (Grond et al, 2017; Hirabayashi et al, 2017; Pichery et al, 2017). Pnpla1 is involved in the transacylation reaction in the final step of acylceramide production (Ohno et al, 2017). However, the phenotypes of these two KO strains differed in several respects. For example, the skin barrier abnormalities exhibited by *Cyp4f39* KO mice were more severe than those of *Pnpla1* KO mice. The TEWL of *Cyp4f39* KO mice was 14.8 times that of WT mice (Figure 2c), while that of *Pnpla1* KO mice was reported to be 3–6 times higher (Grond et al, 2017; Hirabayashi et

al, 2017; Pichery et al, 2017). *Cyp4f39* KO mice lost 33% of their body weight in 7 h (Figure 2b), while *Pnpla1* KO mice lost about 20% over 16 h (Hirabayashi et al, 2017). The SC of *Cyp4f39* KO mice was thickened, but this was accompanied by weak hyperkeratosis (Figure 3). However, more prominent hyperkeratosis and a condensed SC were observed in *Pnpla1* KO mice (Grond et al, 2017; Pichery et al, 2017). Acanthosis in the SS was observed in *Pnpla1* KO mice (Grond et al, 2017; Hirabayashi et al, 2017; Pichery et al, 2017) but not in *Cyp4f39* KO mice (Figure 3). The changes in gene expression also differed between the two strains. In the *Cyp4f39* KO mouse epidermis, *Flg* was upregulated but *Lor* expression was almost unchanged (Figure 6). In *Pnpla1* KO mice, however, expressions of both *Flg* and *Lor* were downregulated (Hirabayashi et al, 2017). The expression levels of *Abca12* were not affected in *Cyp4f39* KO mice (Figure 6), whereas those in *Pnpla1* KO mice were elevated (Grond et al, 2017; Hirabayashi et al, 2017). Although neither strain could produce acylceramides, they accumulated different intermediates: *Cyp4f39* KO mice accumulated ULC ceramides, while *Pnpla1* KO mice accumulated ω-OH (ULC) ceramides (Figure 5) (Grond et al, 2017; Hirabayashi et al, 2017; Pichery et al, 2017). In other words, the key molecular difference between them was the presence or absence of the ω-hydroxyl group in their ULC ceramides. Considering that the skin barrier abnormalities were less severe in the *Pnpla1* KO strain, we speculate that ω-OH ULC ceramides partially compensate for acylceramide functions.

In the present study, we have shown that the introduction of the ω-hydroxyl group by Cyp4f39 into ceramide/acylceramide is extremely important for skin barrier formation. Patients with atopic dermatitis have reduced skin barrier function and lower levels of acylceramide (Ishikawa et al, 2010). In the future, new therapeutic strategies that improve skin barrier function might be useful for treating ichthyosis and atopic dermatitis. For this purpose, it would

be necessary to apply acylceramides or ω-OH ULC ceramides to the skin or to develop an agent that would stimulate an increase in acylceramide production.

MATERIALS AND METHODS

Mice

Cyp4f39 KO mice were generated using the CRISPR/Cas9 system, as detailed in the Supplementary Material and Methods. All animal experiments were approved by the Institutional Animal Care and Use Committee of Hokkaido University and conducted according to institutional guidelines.

Skin permeability assays

TEWL was measured on the backs of E18.5 mice using an AS-VT100RS evaporimeter (Asch Japan, Tokyo, Japan) as described previously (Sassa et al, 2013). Toluidine blue staining was performed by incubating E18.5 mice in 0.1 % (w/v) toluidine blue solution for 30 min, as described previously (Sassa et al, 2013).

Histological analyses

The skin of the E18.5 mice was prepared and analyzed by hematoxylin/eosin staining or transmission electron microscopy, according to methods described previously (Honda et al, 2018; Naganuma et al, 2016).

Lipid analyses

Lipids were analyzed by TLC or LC-MS/MS using an ultra-performance liquid chromatography coupled with triple quadrupole mass spectrometry (Xevo TQ-S; Waters, Milford, MA), as detailed in the Supplementary Material and Methods.

Quantitative RT-PCR

Real-time quantitative RT-PCR was performed using the One Step TB Green PrimeScript RT-PCR Kit II (Takara Bio, Shiga, Japan), as detailed in the Supplementary Material and Methods.

Data availability statement

There are no datasets related to this article.

CONFLICT OF INTEREST

The authors declare no conflict of interest.

ACKNOWLEDGEMENTS

We thank Dr. Yusuke Ohno for technical support. This work was supported by the Advanced Research and Development Programs for Medical Innovation (AMED-CREST) Grant Number JP19gm0910002 (to A.K.) from the Japan Agency for Medical Research and Development (AMED) and by KAKENHI Grant Numbers JP18H03976 (to A.K.) and JP18H04664 (to A.K.) from the Japan Society for the Promotion of Science (JSPS).

CRediT statement

M.M., investigation, formal analysis, validation, and writing; N.I., investigation and formal analysis; M.S., methodology; T.S., supervision; A.K., conceptualization, funding acquisition, project administration, supervision, and writing.

REFERENCES

Aldahmesh MA, Mohamed JY, Alkuraya HS, Verma IC, Puri RD, Alaiya AA, et al. Recessive mutations in *ELOVL4* cause ichthyosis, intellectual disability, and spastic quadriplegia. Am J Hum Genet 2011;89:745-50.

Basel-Vanagaite L, Attia R, Ishida-Yamamoto A, Rainshtein L, Ben Amitai D, Lurie R, et al. Autosomal recessive ichthyosis with hypotrichosis caused by a mutation in *ST14*, encoding type II transmembrane serine protease matriptase. Am J Hum Genet 2007;80:467-77.

Chan A, Mauro T. Acidification in the epidermis and the role of secretory phospholipases. Dermatoendocrinol 2011;3:84-90.

Deraison C, Bonnart C, Lopez F, Besson C, Robinson R, Jayakumar A, et al. LEKTI fragments specifically inhibit KLK5, KLK7, and KLK14 and control desquamation through a pH-dependent interaction. Mol Biol Cell 2007;18:3607-19.

Elias PM, Crumrine D, Rassner U, Hachem JP, Menon GK, Man W, et al. Basis for abnormal desquamation and permeability barrier dysfunction in RXLI. J Invest Dermatol 2004;122:314-9.

Elias PM, Gruber R, Crumrine D, Menon G, Williams ML, Wakefield JS, et al. Formation and functions of the corneocyte lipid envelope (CLE). Biochim Biophys Acta 2014;1841:314-8.

Grond S, Eichmann TO, Dubrac S, Kolb D, Schmuth M, Fischer J, et al. PNPLA1 deficiency in mice and humans leads to a defect in the synthesis of omega-O-acylceramides. J Invest Dermatol 2017;137:394-402.

Hirabayashi T, Anjo T, Kaneko A, Senoo Y, Shibata A, Takama H, et al. PNPLA1 has a crucial role in skin barrier function by directing acylceramide biosynthesis. Nat Commun

2017;8:14609.

Hirabayashi T, Murakami M, Kihara A. The role of PNPLA1 in ω-*O*-acylceramide synthesis and skin barrier function. Biochim Biophys Acta 2019;1864:869-79.

Honda Y, Kitamura T, Naganuma T, Abe T, Ohno Y, Sassa T, et al. Decreased skin barrier lipid acylceramide and differentiation-dependent gene expression in ichthyosis gene *Nipal4*-knockout mice. J Invest Dermatol 2018;138:741-9.

Hotz A, Bourrat E, Küsel J, Oji V, Alter S, Hake L, et al. Mutation update for *CYP4F22* variants associated with autosomal recessive congenital ichthyosis. Hum Mutat 2018;39:1305-13.

Ishida-Yamamoto A, Igawa S. Genetic skin diseases related to desmosomes and corneodesmosomes. J Dermatol Sci 2014;74:99-105.

Ishikawa J, Narita H, Kondo N, Hotta M, Takagi Y, Masukawa Y, et al. Changes in the ceramide profile of atopic dermatitis patients. J Invest Dermatol 2010;130:2511-4.

Jennemann R, Rabionet M, Gorgas K, Epstein S, Dalpke A, Rothermel U, et al. Loss of ceramide synthase 3 causes lethal skin barrier disruption. Hum Mol Genet 2012;21:586-608.

Kihara A. Very long-chain fatty acids: elongation, physiology and related disorders. J Biochem 2012;152:387-95.

Kihara A. Synthesis and degradation pathways, functions, and pathology of ceramides and epidermal acylceramides. Prog Lipid Res 2016;63:50-69.

Krien PM, Kermici M. Evidence for the existence of a self-regulated enzymatic process within the human stratum corneum -an unexpected role for urocanic acid. J Invest Dermatol 2000;115:414-20.

Kutkowska-Kazmierczak A, Rydzanicz M, Chlebowski A, Klosowska-Kosicka K, Mika A,

Gruchota J, et al. Dominant *ELOVL1* mutation causes neurological disorder with ichthyotic keratoderma, spasticity, hypomyelination and dysmorphic features. J Med Genet 2018;55:408-14.

Lefèvre C, Bouadjar B, Ferrand V, Tadini G, Mégarbané A, Lathrop M, et al. Mutations in a new cytochrome P450 gene in lamellar ichthyosis type 3. Hum Mol Genet 2006;15:767-76.

Mueller N, Sassa T, Morales-Gonzalez S, Schneider J, Salchow DJ, Seelow D, et al. De novo mutation in *ELOVL1* causes ichthyosis, *acanthosis nigricans*, hypomyelination, spastic paraplegia, high frequency deafness and optic atrophy. J Med Genet 2019;56:164-75.

Naganuma T, Takagi S, Kanetake T, Kitamura T, Hattori S, Miyakawa T, et al. Disruption of the Sjögren-Larsson syndrome gene *Aldh3a2* in mice increases keratinocyte growth and retards skin barrier recovery. J Biol Chem 2016;291:11676-88.

Narangifard A, den Hollander L, Wennberg CL, Lundborg M, Lindahl E, Iwai I, et al. Human skin barrier formation takes place via a cubic to lamellar lipid phase transition as analyzed by cryo-electron microscopy and EM-simulation. Exp Cell Res 2018;366:139-51.

Ohno Y, Kamiyama N, Nakamichi S, Kihara A. PNPLA1 is a transacylase essential for the generation of the skin barrier lipid ω-*O*-acylceramide. Nat Commun 2017;8:14610.

Ohno Y, Nakamichi S, Ohkuni A, Kamiyama N, Naoe A, Tsujimura H, et al. Essential role of the cytochrome P450 CYP4F22 in the production of acylceramide, the key lipid for skin permeability barrier formation. Proc Natl Acad Sci U S A 2015;112:7707-12.

Ohno Y, Nara A, Nakamichi S, Kihara A. Molecular mechanism of the ichthyosis pathology of Chanarin-Dorfman syndrome: Stimulation of PNPLA1-catalyzed ω-*O*-acylceramide production by ABHD5. J Dermatol Sci 2018;92:245-53.

Oji V, Tadini G, Akiyama M, Blanchet Bardon C, Bodemer C, Bourrat E, et al. Revised nomenclature and classification of inherited ichthyoses: results of the First Ichthyosis Consensus Conference in Soreze 2009. J Am Acad Dermatol 2010;63:607-41.

Pichery M, Huchenq A, Sandhoff R, Severino-Freire M, Zaafouri S, Opalka L, et al. PNPLA1 defects in patients with autosomal recessive congenital ichthyosis and KO mice sustain PNPLA1 irreplaceable function in epidermal omega-O-acylceramide synthesis and skin permeability barrier. Hum Mol Genet 2017;26:1787-800.

Radner FP, Streith IE, Schoiswohl G, Schweiger M, Kumari M, Eichmann TO, et al. Growth retardation, impaired triacylglycerol catabolism, hepatic steatosis, and lethal skin barrier defect in mice lacking comparative gene identification-58 (CGI-58). J Biol Chem 2010;285:7300-11.

Sassa T, Ohno Y, Suzuki S, Nomura T, Nishioka C, Kashiwagi T, et al. Impaired epidermal permeability barrier in mice lacking *Elovl1*, the gene responsible for very-long-chain fatty acid production. Mol Cell Biol 2013;33:2787-96.

Sugiura K, Akiyama M. Update on autosomal recessive congenital ichthyosis: mRNA analysis using hair samples is a powerful tool for genetic diagnosis. J Dermatol Sci 2015;79:4-9.

Vasireddy V, Uchida Y, Salem N, Jr., Kim SY, Mandal MN, Reddy GB, et al. Loss of functional ELOVL4 depletes very long-chain fatty acids (≥C28) and the unique ω-O-acylceramides in skin leading to neonatal death. Hum Mol Genet 2007;16:471-82.

Zheng Y, Yin H, Boeglin WE, Elias PM, Crumrine D, Beier DR, et al. Lipoxygenases mediate the effect of essential fatty acid in skin barrier formation: a proposed role in releasing omega-hydroxyceramide for construction of the corneocyte lipid envelope. J Biol Chem 2011;286:24046-56.

FIGURE LEGENDS

Figure 1. Study background and generation of *Cyp4f39* KO mice. (**a**) Structure of acylceramide. Acylceramides are composed of a long-chain base (blue; mainly sphingosine), a saturated or monounsaturated C30–C36 ULCFA (black), and a linoleic acid moiety (green). (**b**) Phylogenetic tree of human and mouse CYP4F/Cyp4f family members. CYP4F** (all capital letters) and Cyp4f** (only first letter capitalized) indicate human and mouse CYP proteins, respectively. (**c**) The exon structure (red, coding sequences; blue, untranslated regions) of *Cyp4f39* and the nucleotide sequence around the guide RNA target sequence is shown. *Cyp4f39* KO mice have a 32 bp deletion (boxed). The blue and orange nucleotides represent the target sequence and the protospacer-adjacent motif sequence, respectively. (**d**) Photographs of WT and *Cyp4f39* KO mice at E18.5.

Figure 2. Skin barrier abnormalities and neonatal lethality of *Cyp4f39* KO mice. (**a–d**) *Cyp4f39*$^{+/+}$, *Cyp4f39*$^{+/-}$, and *Cyp4f39*$^{-/-}$ mice were prepared by cesarean section at E18.5. (**a, b**) Time courses of survival (**a**) and body weight loss (**b**) of *Cyp4f39*$^{+/+}$ (n = 5), *Cyp4f39*$^{+/-}$ (n = 10), and *Cyp4f39*$^{-/-}$ (n = 4) mice. (**c**) TEWL values for *Cyp4f39*$^{+/+}$ (n = 16), *Cyp4f39*$^{+/-}$ (n = 16), and *Cyp4f39*$^{-/-}$ (n = 12) mice. Values presented in (**b**) and (**c**) are means ± SDs with statistically significant differences indicated. ** $P < 0.01$ (Tukey's test). (**d**) Mice were stained with 0.1% toluidine blue for 30 min and photographed.

Figure 3. Impaired lipid lamellae formation and persistence of periderm in *Cyp4f39* KO mice. (**a–e**) Sections of WT and *Cyp4f39* KO mouse skin at E18.5 were subjected to hematoxylin/eosin staining (**a**) and transmission electron microscopy (**b–e**). (**a**) Bar, 50 μm. (**b**)

The middle and bottom images are enlarged views of the pink rectangles in the top images. The yellow and green arrowheads indicate corneodesmosomes and lamellar bodies, respectively. Bars, 5 μm (top and middle) and 0.5 μm (bottom). PD, periderm; asterisk, unknown structures (possibly artificial deposits). (**c–e**) Lipid lamellae thickness (**c**), number of stratum corneum layers (**d**) and number of corneodesmosomes (**e**) were quantified from ≥10 randomly selected images. Values presented are means ± SDs. ** $P < 0.01$ (Student's *t*-test).

Figure 4. Decreased acylceramide levels in *Cyp4f39* KO mice. (**a, b**) Lipids were extracted from the epidermis of WT (n = 3) and *Cyp4f39* KO mice (n = 3) at E18.5. (**a**) Lipids were separated by TLC and stained with copper phosphate. (**b**) Acylceramides were quantified using LC-MS/MS. The left panel shows the quantity of each acylceramide species, which are distinguished according to chain length and the degree of saturation of the FA moiety, and the right panel shows the total quantity of acylceramides. Values represent means ± SDs. Statistically significant differences are indicated. ** $P < 0.01$ (Student's *t*-test). OAHFA, *O*-acyl ω-OH FA; Chol, cholesterol; Acyl-Cer, acylceramide; Cer, ceramide; Acyl-GlcCer, acyl-glucosylceramide; GlcCer, glucosylceramide; GPL, glycerophospholipid; LC, long-chain; VLC, very-long-chain; n.d., not detected.

Figure 5. Decreased ω-OH ceramide levels and increased ULC ceramide levels in *Cyp4f39* KO mice. (**a, c**) Structures of ω-OH ceramide (**a**) and ceramide (**c**). (**b**, **d**) Lipids were extracted from the epidermis of WT (n = 3) and *Cyp4f39* KO mice (n = 3) at E18.5, and ω-OH ceramides (**b**) and ceramides (**d**) were quantified using LC-MS/MS. The left-hand graph in (**b**) and the graph in (**d**) show the quantity of each ω-OH ceramide and ceramide species. The right-

hand graph in (**b**) indicates the total quantities of ω-OH ceramides. Values present means ± SDs. Statistically significant differences are indicated * $P < 0.05$, ** $P < 0.01$ (Student's *t*-test).

Figure 6. Effects of *Cyp4f39* disruption on expressions of keratinocyte-differentiation markers and acylceramide synthesis genes. Total mRNAs were extracted from the epidermis of WT (n = 3) and *Cyp4f39* KO (n = 3) mice at E18.5, and expression levels of the genes involved in cytoskeleton formation (*Krt14*, *Krt10*, and *Flg*), cornified envelope formation (*Lor* and *Ivl*), acylceramide synthesis (*Elovl1*, *Elovl4*, *Cers3*, *Pnpla1*, and *Abhd5*), lamellar body formation (*Abca12*), and protein-bound ceramide synthesis (*Aloxe3*), as well as that of the housekeeping gene (*Hprt*), were examined by quantitative real-time RT-PCR. Values are expressed relative to *Hprt* and represent means ± SDs. Statistically significant differences are indicated. * $P < 0.05$ (Student's *t*-test).

SUPPLEMENTARY MATERIAL

SUPPLEMENTARY MATERIAL AND METHODS

Breeding of mice and generation of *Cyp4f39* KO mice

C57BL/6J mice were used as WT mice. *Cyp4f39* KO mice were generated using the CRISPR/Cas9 system as follows. The guide RNA targeted the 23 bases adjacent to the protospacer-adjacent motif sequence in exon 11 of *Cyp4f39*, and a primer pair (f1 and f2; Supplementary Table S1) containing them was annealed and cloned into the *Bbs*I site of the CRISPR/Cas9 vector pX330 (Addgene, Watertown, MA). The resulting plasmid was injected into fertilized eggs of C57BL/6J mice. Genomic DNAs were prepared from the tails of offspring and subjected to PCR using primers p1 and p2 (Supplementary Table S1) to amplify the target sequence and carry out subsequent DNA sequencing. One of the mice had a deletion of 32 bp and was used for further analyses. *Cyp4f39* heterozygous KO mice were maintained by back-crossing with C57BL/6J mice. *Cyp4f39* homozygous KO mice were obtained by crossing the *Cyp4f39* heterozygous KO mice. Mouse genotypes were determined by PCR using genomic DNAs and primers p1 and p2, followed by DNA cleavage with the restriction enzyme *Afl*III and electrophoresis.

Mice were housed under specific pathogen-free conditions at a room temperature of 23 ± 1 °C and humidity of 50 ± 5%, with a 12 h light/dark cycle and food and water available *ad libitum*. Female mice were housed with male mice overnight to allow mating. Noon of the next day was set as E0.5. Neonatal mice were prepared by cesarean section at E18.5 and used for analyses.

Lipid analyses

Skin prepared from the backs of E18.5 mice was incubated with 600 μL of PBS at 55 °C for 3 min, and then separated into epidermis and dermis. The epidermis (10–20 mg) was transferred to a homogenizer, mixed with 2 mL of chloroform/methanol/water (30:60:8, v/v/v), and homogenized for ~10 min. After incubation at 50 °C for 15 min, samples were centrifuged at 800 × g for 15 min, and the supernatant was collected. The extraction procedure was repeated three times, and the supernatants were combined. Phase separation was performed by addition of 4.8 mL of water and subsequent centrifugation at 800 × g for 15 min. The supernatant was dried, suspended in chloroform/methanol (2:1, v/v), and analyzed by TLC or LC-MS/MS as follows.

Lipids corresponding to 1 mg of epidermis were separated using normal-phase TLC plates (Silica gel 60; Merck Millipore, Darmstadt, Germany) using the following three solvent systems: (1) chloroform/methanol/water (40:10:1, v/v), developed to 2 cm from the bottom, dried, and developed again to 5 cm from the bottom; (2) chloroform/methanol/acetic acid (47:2:0.5, v/v), developed to 1.5 cm from the top; and (3) hexane/diethylether/acetic acid (65:35:1, v/v), developed to 0.5 cm from the top. Lipids were detected by spraying with a copper phosphate reagent [3% $CuSO_4$ (w/v) in 8 % (v/v) aqueous phosphoric acid solution] and heating at 180 °C for 3 min.

Lipids corresponding to 125 ng of epidermis were subjected to LC-MS/MS analysis using an ultra-performance liquid chromatography coupled with triple quadrupole mass spectrometry (Xevo TQ-S; Waters), as described previously (Honda et al, 2018; Ohno et al, 2017). Lipids were separated using a reversed-phase column (Acquity UPLC CSH C18 column; particle size, 1.7 μm; inner diameter, 2.1 mm; length, 100 mm; Waters). Ionization was performed using the electrospray ionization method, and acylceramides, ceramides, and ω-OH ceramides were detected by MS/MS in multiple reaction monitoring mode. The values of the mass-to-charge

(*m/z*) ratio set at quadrupole mass filters Q1 and Q3 (specific to each lipid species), the cone voltages, and the collision energies used are as described previously (Honda et al, 2018).

Quantitative RT-PCR

Skin prepared from the E18.5 mice was incubated with PBS at 55 ℃ for 3 min and then separated into epidermis and dermis. Total RNA was prepared using the NucleoSpin RNA II kit (Takara Bio). Real-time quantitative RT-PCR was performed using 50 ng/μL of total RNA, primers (Supplementary Table S1), and the One Step TB Green PrimeScript RT-PCR Kit II (Takara Bio). Reactions were performed on the CFX96 Touch Real-Time PCR Detection System (Bio-Rad, Hercules, CA). The reaction was conducted by incubating the samples at 50 ℃ for 30 min and 94 ℃ for 2 min, followed by 35 cycles of 94 ℃ for 30 s, 60 ℃ for 30 s, and 72 ℃ for 1 min. mRNA levels were normalized with respect to *Hprt*.

SUPPLEMENTARY REFERENCES

Honda Y, Kitamura T, Naganuma T, Abe T, Ohno Y, Sassa T, et al. Decreased skin barrier lipid acylceramide and differentiation-dependent gene expression in ichthyosis gene *Nipal4*-knockout mice. J Invest Dermatol 2018;138:741-9.

Ohno Y, Kamiyama N, Nakamichi S, Kihara A. PNPLA1 is a transacylase essential for the generation of the skin barrier lipid ω-*O*-acylceramide. Nat Commun 2017;8:14610.

SUPPLEMENTARY FIGURE LEGEND

Figure S1. Synthetic pathway of acylceramide and protein-bound ceramide. Intermediates, reactions, and genes involved are also shown. From the upper stratum spinosum to the stratum granulosum, acylceramide is synthesized, glucosylated, and stored in lamellar granules (lamellar bodies). At the boundary between the stratum granulosum and the stratum corneum, these lamellar bodies fuse with the cell membrane, and the stored acyl-glucosylceramide is released extracellularly. This acyl-glucosylceramide is then converted back into acylceramide in the lipid lamellae. However, some of the acylceramide is converted into protein-bound ceramide through modification of its linoleic acid moiety, subsequent hydrolysis, and covalent bonding with corneocyte surface proteins. LC, long-chain.

Figure S2. Magnifications of the periderm and corneodesmosomes in *Cyp4f39* KO mouse epidermis. (**a** and **b**) Skin sections from a WT (**b**) and a *Cyp4f39* KO mouse (**a** and **b**) at E18.5 were subjected to transmission electron microscopy analysis. The right-hand images are enlarged views of the areas in pink rectangles in the left-hand images. The yellow arrowheads indicate corneodesmosomes. Bars, 5 μm (left) and 1 μm (right). PD, periderm.

Figure 1

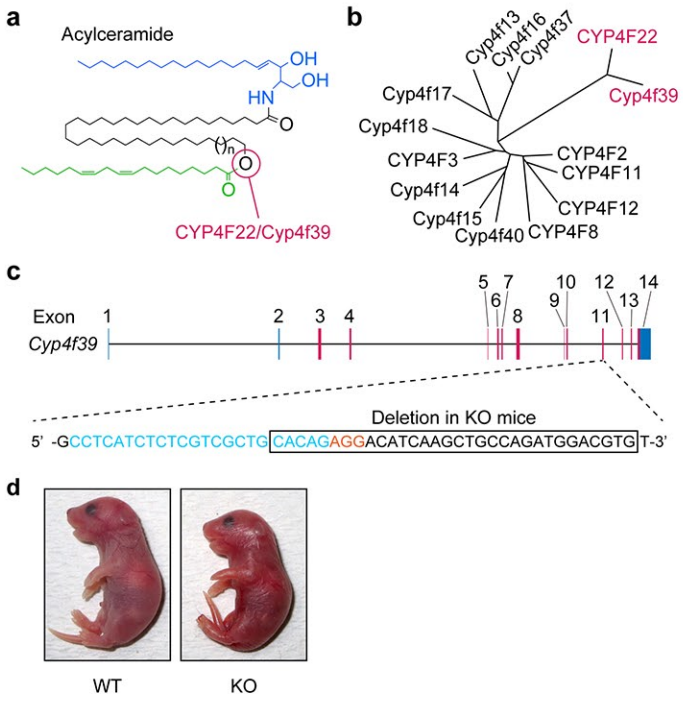
a
Acylceramide
OH
OH
HN
O
n
O
O
CYP4F22/Cyp4f39
b
Cyp4f13
Cyp4f16
Cyp4f37
CYP4F22
Cyp4f39
Cyp4f17
Cyp4f18
CYP4F3
CYP4F2
CYP4F11
Cyp4f14
CYP4F12
Cyp4f15
Cyp4f40
CYP4F8
c
Exon 1 2 3 4 5 6 7 8 9 10 11 12 13 14
Cyp4f39
Deletion in KO mice
5' -GCCTCATCTCTCGTCGCTGCACAGAGGACATCAAGCTGCCAGATGGACGTGT-3'
d
WT
KO

Figure 2

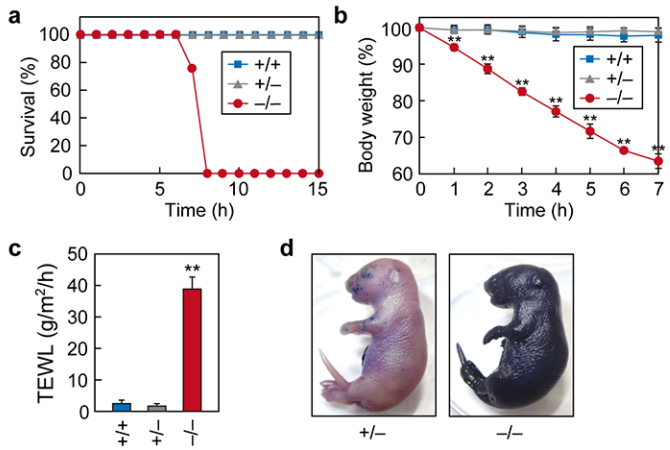
a
Survival (%)
100
80
60
40
20
0
0
5
10
15
Time (h)
+/+
+/–
–/–
b
Body weight (%)
100
90
80
70
60
0
1
2
3
4
5
6
7
Time (h)
**
+/+
+/–
–/–
c
TEWL (g/m²/h)
50
40
30
20
10
0
**
+/+
+/–
–/–
d
+/–
–/–

Figure 3

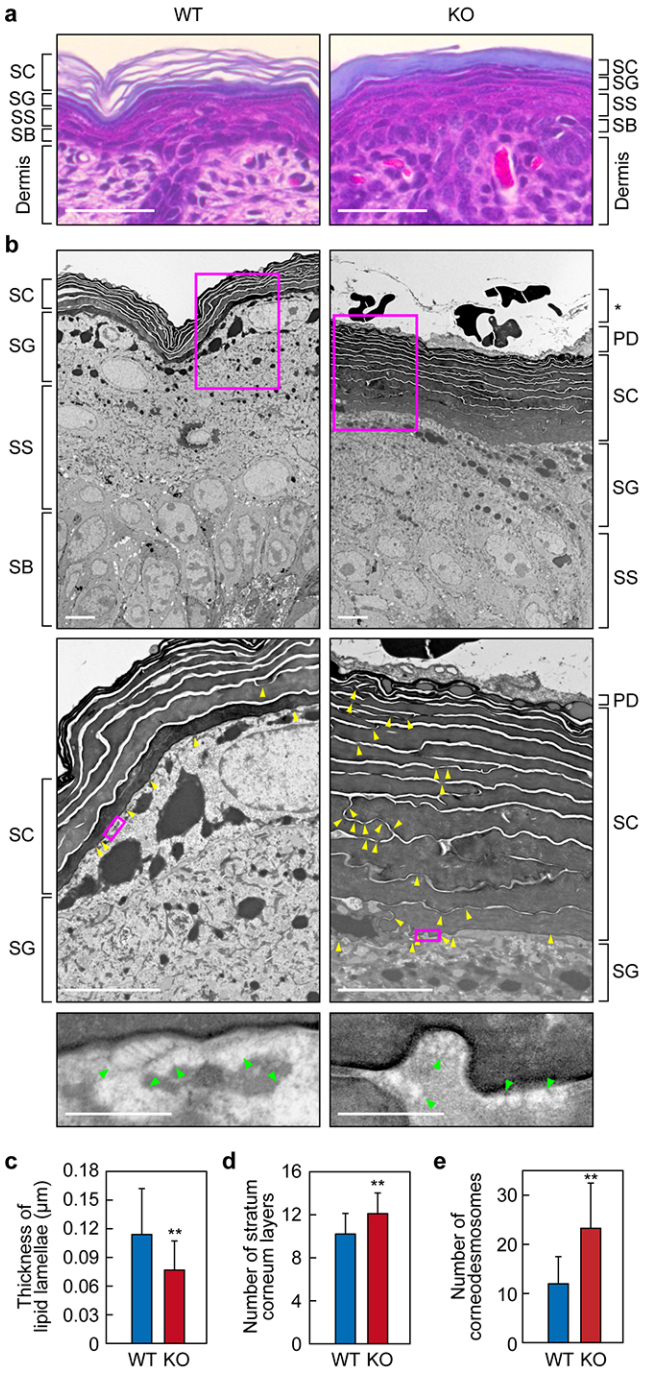
a
WT
KO
SC
SG
SS
SB
Dermis
b
*
PD
c
Thickness of lipid lamellae (μm)
0.18
0.15
0.12
0.09
0.06
0.03
0
**
WT KO
d
Number of stratum corneum layers
16
12
8
4
0
**
WT KO
e
Number of corneodesmosomes
30
20
10
0
**
WT KO

Figure 4

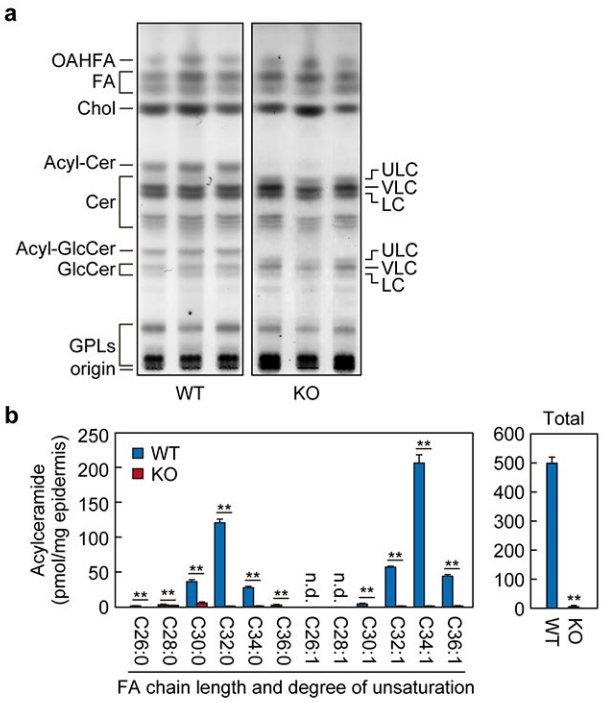
a
OAHFA
FA
Chol
Acyl-Cer
Cer
Acyl-GlcCer
GlcCer
GPLs
origin
ULC
VLC
LC
ULC
VLC
LC
WT
KO
b
Acylceramide (pmol/mg epidermis)
WT
KO
250
200
150
100
50
0
**
n.d.
C26:0
C28:0
C30:0
C32:0
C34:0
C36:0
C26:1
C28:1
C30:1
C32:1
C34:1
C36:1
FA chain length and degree of unsaturation
Total
600
500
400
300
200
100
0
WT
KO

Figure 5

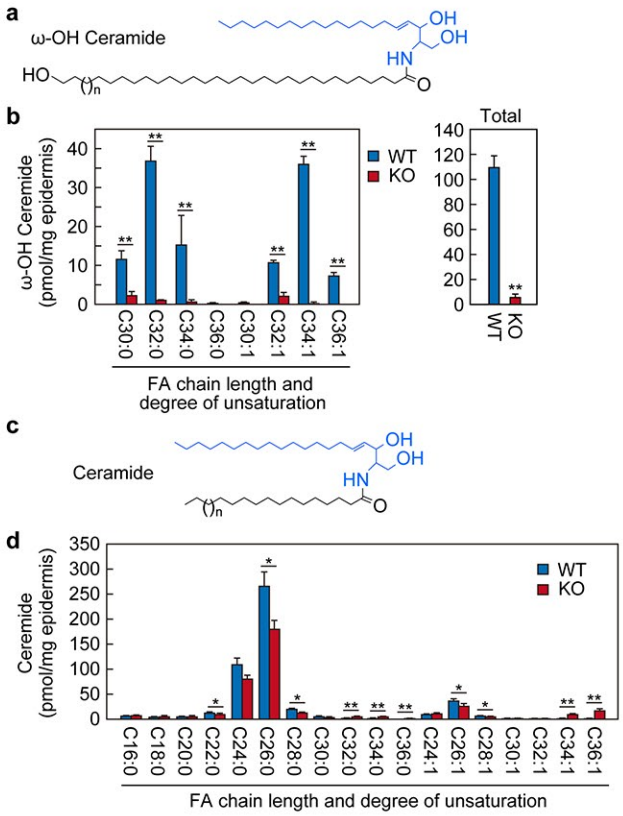
a
ω-OH Ceramide
OH
OH
HN
HO
O
b
ω-OH Ceremide (pmol/mg epidermis)
WT
KO
Total
C30:0
C32:0
C34:0
C36:0
C30:1
C32:1
C34:1
C36:1
FA chain length and degree of unsaturation
c
Ceramide
d
Ceremide (pmol/mg epidermis)
C16:0
C18:0
C20:0
C22:0
C24:0
C26:0
C28:0
C30:0
C32:0
C34:0
C36:0
C24:1
C26:1
C28:1
C30:1
C32:1
C34:1
C36:1
FA chain length and degree of unsaturation

Figure 6

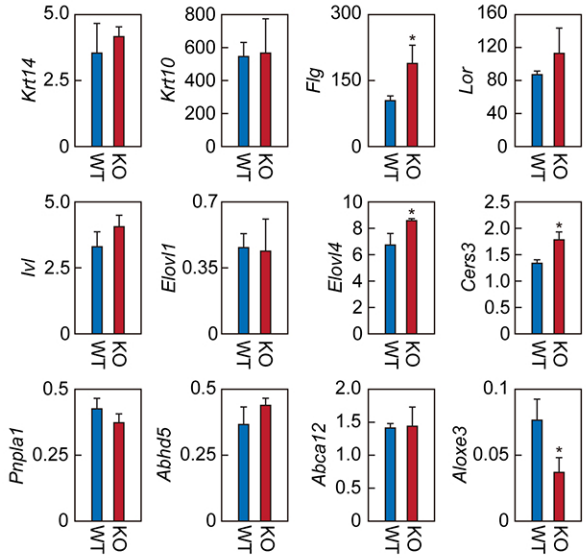
Krt14
5.0
2.5
0
WT
KO
Krt10
800
600
400
200
0
Flg
300
150
*
Lor
160
120
80
40
Ivl
0.7
0.35
Elovl1
10
8
6
4
2
Elovl4
2.5
2.0
1.5
1.0
0.5
Cers3
Pnpla1
0.25
Abhd5
Abca12
0.1
0.05
Aloxe3

Figure S1

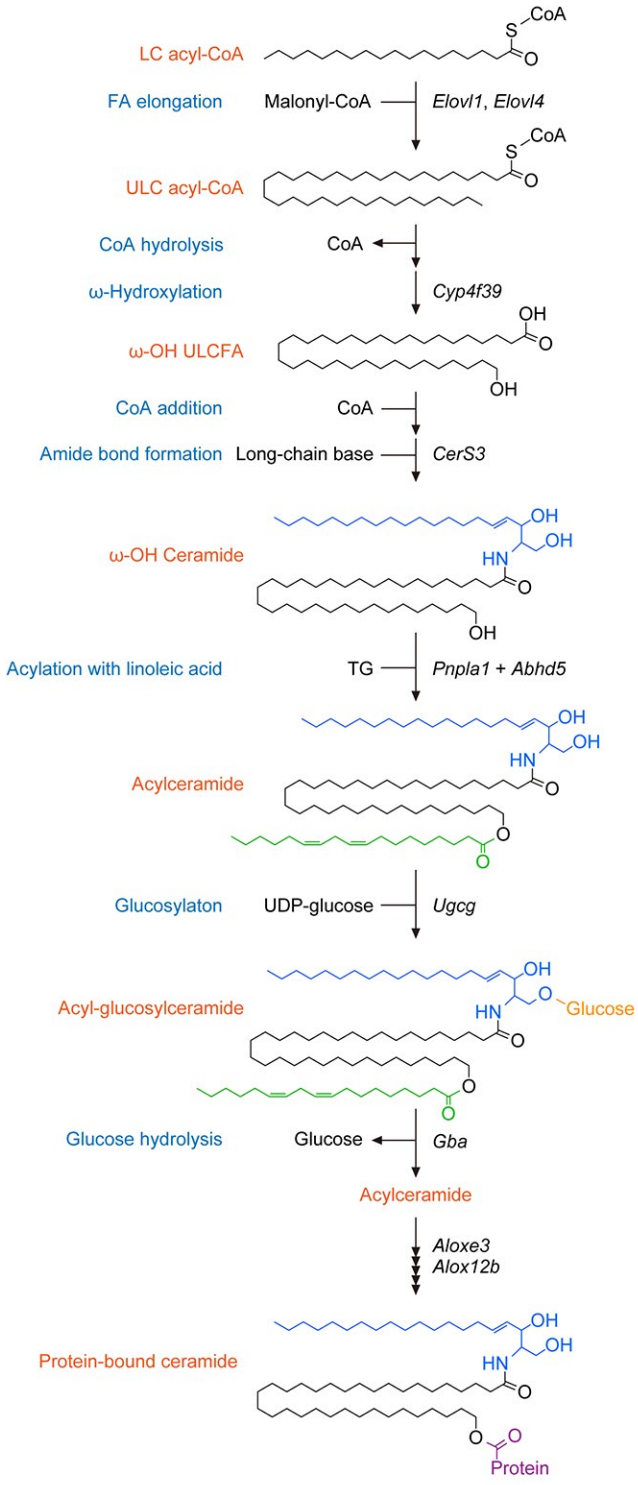
LC acyl-CoA
FA elongation
Malonyl-CoA
Elovl1, Elovl4
ULC acyl-CoA
CoA hydrolysis
CoA
ω-Hydroxylation
Cyp4f39
ω-OH ULCFA
CoA addition
CoA
Amide bond formation
Long-chain base
CerS3
ω-OH Ceramide
Acylation with linoleic acid
TG
Pnpla1 + Abhd5
Acylceramide
Glucosylaton
UDP-glucose
Ugcg
Acyl-glucosylceramide
Glucose
Glucose hydrolysis
Glucose
Gba
Acylceramide
Aloxe3
Alox12b
Protein-bound ceramide
Protein

Figure S2